[American Journal of Science, Vol. 317, Month, 2017, P. 000–000, DOI 10.2475/●]

THE WATER-CARBON DIOXIDE MISCIBILITY SURFACE TO 450 °C AND 7 GPa

EVAN H. ABRAMSON†, OLIVIER BOLLENGIER, and J. MICHAEL BROWN

ABSTRACT. Fluid-fluid immiscibility in the water-carbon dioxide binary system has been measured to a pressure of 7 GPa and temperature of 450 °C, providing the first such data under conditions overlapping those found in subduction zones and the icy worlds of the outer solar system. Water and carbon dioxide were loaded as inhomogeneous mixtures in externally-heated diamond-anvil cells. Mole fractions were determined by isotopic doping of the initial constituents followed by measurement of the equilibrated isotopic content of the decanted samples. Homogenization and dehomogenization of fluids were observed visually for mole fractions of carbon dioxide from 20 to 90 percent. The recorded pressure-temperature points of homogenization were inverted to give a miscibility surface. The path of the critical curve continues to the highest pressures measured, with no indication of an upper critical endpoint. For mole fractions of carbon dioxide less than 40 percent, the minimum temperature necessary to form a homogeneous solution decreases sharply above a compositionally-dependent pressure. Based on measured intensities of Raman lines, this behavior is linked to a change in speciation as the equilibrium shifts from dissolved carbon dioxide to, presumably, either bicarbonate ion or carbonic acid. Published equations of state give poor representations of the miscibility surface, neither the abrupt behavior due to speciation nor the critical curves being correctly predicted. The experimental constraints provided by the current data should allow useful refinements of equations of state over a wide pressure-temperature-compositional space where only extrapolations and molecular dynamic simulations were previously available. Improved equations of state are a prerequisite for better geochemical models for Earth and extraterrestrial ocean worlds.

Key words: carbon dioxide, water, miscibility, high pressure, diamond anvil, phase diagram, speciation

INTRODUCTION

Carbon dioxide and water are primary constituents of fluid mixtures in the crust and mantle of Earth as well as in the interiors of several outer solar system icy worlds (Porco and others, 2006; McCord and others, 2008). These fluids are responsible for the transport and concentration of soluble chemical species, mediate the chemical reactivity of rocks (depressing melting points of silicates, and allowing hydration/dehydration and carbonization/decarbonization reactions), alter the rheology of rocks, and are implicated in processes associated with subduction zone tremor (Audet and others, 2010) and deep earthquakes (Abers and others, 2013).

Aqueous solutions of carbon dioxide are particularly important vehicles for carbon transport and likely influence the fate of carbon during subduction (for example, Hirschmann and Dasgupta, 2009; Sverjensky and others, 2014a; Kelemen and Manning, 2015). Fluid paths through, along, and out of the slab (see fig. 1 for estimated subduction zone geotherms) govern the degree to which carbon is either conducted into the deep mantle or rapidly re-cycled to the surface. Thus, these fluids may be considered gatekeepers in the "carbon cycle."

In the aqueous environments inside large icy worlds the high-pressure solubilities of CO_2 additionally affect the fluid solidus and the evolution of hydrates. Gas hydrates

Department of Earth and Space Sciences, University of Washington, Seattle, Washington 98195-1310 USA; obollengier@gmail.com; brown@ess.washington.edu
† Corresponding author: evan@ess.washington.edu

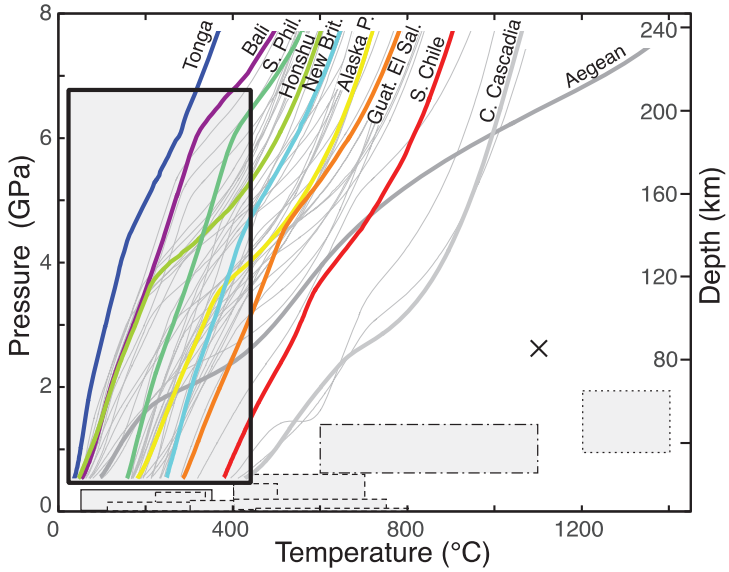

Fig. 1. Temperatures and pressures of the subducting Moho (7 km under the plate interface), as given by model W1300 of Syracuse and others, 2010, with several segments labeled (thicker curves), most not. Overlaid rectangles demark regions in which data exist for the H_2O-CO_2 system; of particular note: current study (thicker, solid border); Todheide and Franck, 1963, thinner solid border; Aranovich and Newton, 1999, dot and dash border; Frost and Wood, 1997, dotted border; Eggler and others, 1979, x; all others, dashed border.

are expected to be major factors in the thermo-chemical evolution of icy moons such as Ganymede or Titan (Sohl and others, 2010).

In order to understand processes associated with H_2O-CO_2 fluids, their thermodynamic properties are required within the relevant ranges of pressure, temperature and concentration. Inclusions in diamonds, and in crystals extracted from xenoliths, suggest such fluids extend well into Earth's mantle, to pressures exceeding 10 GPa (Harte, 2010), and that fluid compositions can range from water-rich to CO_2-rich (Andersen and Neumann, 2001). The lowest temperatures at depth, associated with rapid subduction of old oceanic lithosphere, have been estimated by Syracuse and others, 2010, to lie near 400 °C at a depth of 240 km and pressure of 8 GPa (fig. 1). This implied average thermal gradient (1.7 °C-km^{-1}) is significantly lower than a commonly assumed lower limit for terrestrial metamorphic conditions of 5 °C-km^{-1} (for example, Frost and Frost, 2014). Even lower temperatures at pressure pertain to the icy worlds of the outer solar system; for example, the Ganymede ocean-silicate interface near 1.5 GPa lies within the temperature stability regime of high pressure water ices (Vance and others, 2014). At somewhat lower pressures, H_2O-CO_2 fluids are also of potential industrial interest. Oil and gas wells, for instance, now commonly reach pressures in excess of 100 MPa, and at least one exploration well has been reported at 180 MPa (Shadravan and Amani, 2012). Further, both water and carbon dioxide are inexpensive and non-toxic solvents; industrial processes may be envisioned which would profit from these desirable traits coupled with the tunability of mixed-solvent properties through variation of pressure, temperature and mixing ratios. These processes are most likely to be economically undertaken at intermediate pressures up to 500 MPa (Vetter, 2001).

Despite the wide applicability of thermodynamic data, the difficulties associated with studying mixed fluids of water and carbon dioxide are such that almost all

previously reported experiments pertain to pressures lower than 1 GPa, most of them below 600 MPa (see fig. 1, and tabulations in Mader, 1991, and in Duan and Zhang, 2006). Exceptions are the work of Eggler and others, 1979, conducted at 2.6 GPa, that of Frost and Wood, 1997, which was limited to a maximum pressure of 2 GPa, and of Aranovich and Newton, 1999, to 1.4 GPa. Furthermore, even well inside the explored regime, at moderately low (~80 MPa) pressures relevant to geothermal engineering, significant disagreement on solubilities of water in CO_2 remain (Capobianco and others, 2013).

Exploration of the high-pressure fluid-fluid phase diagram, in particular, has extended to 350 MPa (Todheide and Franck, 1963) and 300 MPa (Takenouchi and Kennedy, 1964). Those two studies noted a saddle point in the miscibility surface (corresponding to a minimum temperature in the critical curve) at approximately 200 MPa, 266 °C, and mole fraction CO_2 (X_{CO2}) of 30 to 40 percent. Beyond this minimum, the temperature above which the fluids are infinitely miscibile was seen to rise with pressure, but how far it might continue to do so had not been further addressed. Models of the mixed fluids during subduction or other deep-Earth processes have therefore relied either on extrapolations of low pressure data or on molecular dynamic simulations.

Here we present data on the fluid-fluid miscibilities of the H_2O-CO_2 system up to a pressure of 7 GPa and temperature of 450 °C. Current data, in a range of pressures and temperatures pertinent to conditions in subduction zones, demonstrate that a two-fluid regime extends to the maximum conditions explored. A miscibility surface calculated on the basis of these new data is in substantial conflict with predictions, requiring adjustments of models used in this regime. The current data also indicate the importance of a molecular speciation that varies with pressure, temperature, and composition (PTX), an equilibrium not encompassed by most models.

An equation-of-state (EOS) that correctly reproduces the lower pressure data as well as those of the current study is likely to improve our understanding of fluids within the range of the data, to interpolate well into the economically important, intermediate regime of pressures, and, if partially based on theory, to provide a better grounding for extrapolation to conditions pertinent to higher-temperature rock-fluid interactions.

The paper is organized as follows: the Experimental section contains a brief explanation of sample loading, the measurement of pressure and temperature, and the observation of homogenization (and de-homogenization) of the fluids; additionally, we describe, in detail, a new technique for analyzing the ratios of water to carbon dioxide loaded into the diamond-anvil cell. We then introduce the acquired data, and describe a typical, experimental run. In the Results section we describe the systematics of the observed pressures of homogenization (as functions of temperature), and their inversion to produce a miscibility surface. Following that, the Discussion contains an analysis of the miscibility surface in terms of shifting speciation, compares it with surfaces generated from several equations of state to be found in the literature, and similarly compares the measured critical curve with those generated from published EOS. Finally, we take account of the known solid phases of the system to produce a general, high-pressure P-T-X diagram.

EXPERIMENTAL

Load Preparation

Modified Merrill-Bassett diamond-anvil cells (DACs) were used with rhenium gaskets, the central cavity being lined with gold. Gaskets of hardened Inconel 718, Hastelloy C-276 and 316 stainless steel were all found to corrode at the conditions of these experiments. Carbon dioxide, specified as 99.995 percent pure, was obtained

from Praxair. For the purpose of determining the ratio of water to carbon dioxide loaded into the DACs (see below) water was usually supplied as a dilute (0.055 mol-kg^{-1}) solution of sodium bicarbonate. When loading, the open DAC was first immersed in the solution and a partial vacuum briefly drawn. Release back to atmospheric pressure resulted in a load consisting of solution (without alteration of concentration) and a bubble of air. The cells were sealed and transferred to a pressure vessel. Liquid CO_2 at 10 °C and 5.8 MPa was admitted into the pressure vessel. The immersed DACs were briefly re-opened to allow liquid CO_2 to displace the air, and then re-sealed.

When the cell containing solution and an air bubble is first dried, bicarbonate salt can accumulate around the exteriors of the diamonds and is probably concentrated at the join of diamond and gasket, drawn in by surface tension. Opening such a load to the CO_2 can result in an unknown, but significant, quantity of salt crystals being drawn into the cell. Thus, between the initial loading of the solution and the subsequent loading of CO_2, the sealed cell was dried under vacuum, washed in 0.2 mol-kg^{-1} aqueous HCl during which time a vacuum was repeatedly drawn on the solution, again dried under vacuum, then placed in an ultrasonic bath of de-ionized water for an hour. Additionally, before loading, any fracture found in the indented rhenium gasket along the diamond pavilion was filled with gold to avoid it becoming an unintended reservoir of material.

Measuring Pressure and Temperature

The DAC was placed in an oven with fore and aft optical access. Pressure was determined with a precision of roughly 0.1 GPa (rms scatter of 0.05 GPa) from the Raman spectra of one or more crystals of cubic boron nitride placed inside the DAC (Abramson, 2017), stimulated with 20mW of 488 nm laser light (Ar^+). The back-scattered radiation was collected by a microscope objective of 0.28 numerical aperture and 33.5 mm working distance, and dispersed by a 300 mm monochromator with 1800 lines/mm grating. Spectra were typically acquired over an interval of 30 s. Temperature was monitored with type K thermocouples attached near the diamond culets. At the melting point of lead (Pb), 327.45 °C (McLaren and Murdock, 1960), the reading was off by 1.5 °C, presumably due to gradients through the cell. Sample temperatures were corrected, assuming the difference between the thermocouple reading and sample temperature to be proportional to the difference from ambient temperature. The maximum correction (at our highest temperature of 450 °C) is less than 2 °C.

Determination of Homogenization

Transitions between a homogeneous and an inhomogeneous fluid were determined visually. The contents of the DAC were illuminated from the rear, transmitted light being imaged onto a CCD camera through the same lens as used to collect Raman scatter, followed by a 50 percent reflectance pellicle beamsplitter. A long-pass optical filter between the (incandescent) light and the cell allowed the sample to be observed while Raman spectra were being taken. At a given pressure, temperature was first raised until the load was seen to be homogeneous, then lowered until the re-appearance of a second phase. These temperatures of transition were recorded, the pressure raised, and the process repeated.

The exact temperature of homogenization can be difficult to determine, particularly if the minority phase is adjacent to (and partially obscured by) the gasket. For most loads the de-homogenization (known also as unmixing, or de-mixing) was far more obvious, manifested by the sudden appearance of many small bubbles of minority phase distributed throughout the load (fig. 2). De-homogenization of loads with high X_{CO2} (for example, 89%) proved more difficult to observe as the minority, aqueous, phase tends to wet any pieces of debris on the diamond surfaces rather than

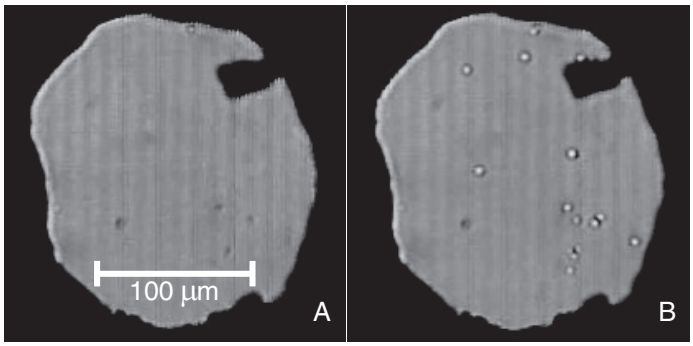

Fig. 2. De-homogenization at 265°C, 2.7 GPa and X_{CO2} = 19%. (A) homogeneous fluid; (B) less than 1°C below the temperature of de-homogenization. The image on the CCD is deliberately de-focused to enhance the contrast between bubbles of minority phase and the bulk fluid.

produce obvious bubbles. Analogous problems in observation of small amounts of aqueous fluid have been remarked in experiments that involved synthetic inclusions homogenizing into a vapor phase (Bodnar and others, 1985; Sterner and Bodnar, 1991). None-the-less, the reproducibility of the measurements and, for the 89 percent load, the straight line paralleling other data (see below, fig. 6C), demonstrate that the points of homogenization are correctly determined.

Observations of homogenization and of de-homogenization produced results identical within the expected uncertainties of pressure and temperature; no metastability with respect to de-homogenization (into two fluids) was ever observed. Particularly for measurements at lower X_{CO2}, and in the absence of pressure drift, the temperatures of transition could be reproducibly measured to 0.1 °C.

Although we did not specifically seek the exact critical conditions for any load, several examples of critical opalescence were observed (fig. 3). Proximity to the critical curve was also evidenced by the temporal behavior of the fluids on a coarser scale, as the regions of different composition move, dissolve and re-appear rapidly.

Measuring Mole Fractions

At sufficiently high pressures and temperatures (for example, 200 MPa, 300 °C) bulk homogeneous CO_2-H_2O solutions might be loaded into the DAC, as was done

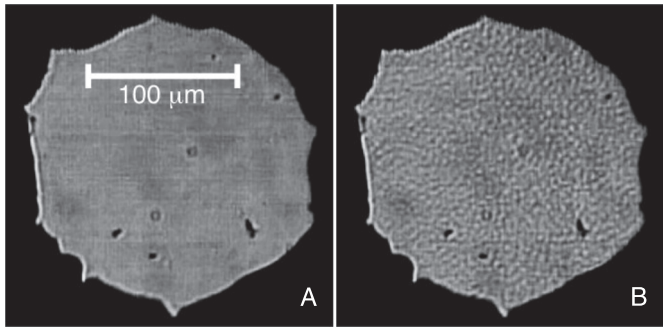

Fig. 3. Critical opalescence at 373 °C, 3.9 GPa, and X_{CO2} = 57%. (A) the homogeneous fluid just above the critical temperature; (B) at the critical temperature. The mottling is on a scale of ~3 μm and could be seen to shimmer. Edge sharpening was applied identically to both images. Persistent dark spots are pieces of spalled gasket.

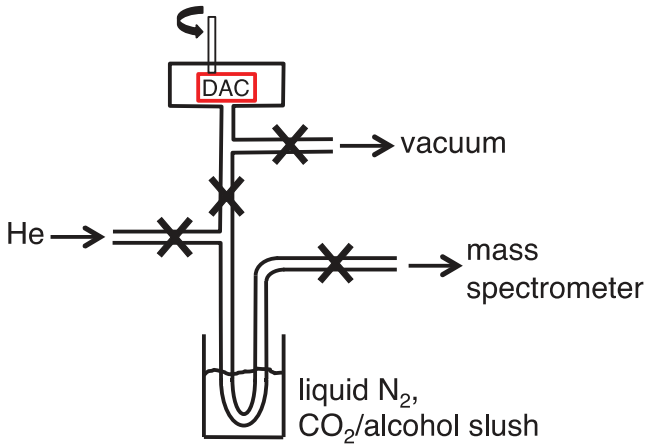

Fig. 4. Diagram of a system for extracting the contents of a DAC into a mass spectrometer. Large crosses denote valves.

with the system N_2-H_2O (Costantino and Rice, 1991; van Hinsberg and others, 1993). However, due to the cost of the required machinery, concerns of safety, and the extremely corrosive properties of CO_2-H_2O solutions, it is desirable to load at lower pressures and temperatures. This then requires a method of determining the resultant mole fractions of the two, immiscible and separately loaded, components. Approximate values can be estimated by visual observation, but we wished to develop a method capable of greater accuracy. The method chosen was to dope the water isotopically, both with ^{18}O and ^{13}C, the latter through use of 0.055 mol-kg^{-1} $NaH^{13}CO_3$ (0.001 mole $NaH^{13}CO_3$/mole H_2O). Isotopic transfer to CO_2, measured at the end of the experiment, can then be related to the loaded X_{CO2}.

In solution, there is rapid exchange between bicarbonate and dissolved CO_2 and thus equilibration of the carbon isotopes. Equilibration of oxygen between water and CO_2 will also be rapid (Poulton and Baldwin, 1967), certainly on the time (and length) scale of our experiments, in which both CO_2 and H_2O are in the fluid state at least 5 hours.

After the observations of homogenization are completed the load is cooled with consequent freezing of both the CO_2 and water; pressure is then brought to roughly 2 GPa. The DAC is placed in an extractor (fig. 4) which is baked to 160 °C under vacuum (<0.3 Pa) for 4 hours. A typical DAC load contains approximately 10 to 100 nmole of analyte, making a thorough de-gassing of the DAC and extractor (fitted with Viton o-ring seals) imperative. Inside the extractor, and after cooling to room temperature, the cell is opened by a wrench on a rotary feedthrough. The gases from the cell expand into an evacuated tube of 316 stainless steel with 4.5 mm ID, and are rapidly trapped in a U bend immersed in liquid nitrogen. The tube is then swept with a flow of He and the liquid nitrogen replaced with an alcohol-CO_2(*s*) slush, allowing the extracted CO_2 to sublime while retaining the water as a solid. The He flow is directed into a Thermo Finnigan MAT 253 continuous flow, isotope ratio, mass spectrometer.

Composition of initial fluids.—Isotopically enriched water (with a stated 1.48 mole% ^{18}O) and bicarbonate (99%^{13}C) were purchased from Icon Isotopes. In order to determine the ^{18}O and ^{17}O content of the purchased enriched water, a sample was diluted with a laboratory standard deionized water of a known isotopic composition ($\delta^{18}O = -10.55$ VSMOW; $\delta^{17}O = -5.55$ VSMOW) to give a ^{18}O content of about $\delta^{18}O = +40$ VSMOW. One gram of the diluted sample was then allowed to equilibrate

at 24 °C with 11 mL of gaseous CO_2 (at 1 bar) of known isotopic content. A sample of the gas was then extracted and analyzed. Adjusting for the additional oxygen from the CO_2, and using equilibrium fractionation values for the $CO_2(g)$-$H_2O(l)$ equilibrium of $\alpha_{18} = 1.041$ and $\alpha_{17} = 1.021$ (Barkan and Luz, 2012), the isotopic content of the purchased water was calculated to be 1.47 percent ^{18}O and 0.095 percent ^{17}O.

The DAC was loaded with a solution made by dilution of the enriched water (with de-ionized tap water) to 0.404 percent ^{18}O (and 0.046% ^{17}O) and addition of bicarbonate to 0.055 mol-kg^{-1}. The liquid carbon dioxide was derived from a petrochemical source with $\delta^{13}C = -36.25$ (VPDB) and $\delta^{18}O = +10.72$ (VSMOW).

Consideration of isotopic fractionation.—In the case of carbon, there is no significant chemical fractionation, as virtually all is released as carbon dioxide. For oxygen, we must consider the possibility of a significant shift from the presumed "random" distribution between CO_2 and water due to the greater affinity of ^{18}O for the former. At 1 bar the fractionation factor between gaseous CO_2 and liquid water is 1.040 (40 ppt) at 21 °C and it decreases with increasing temperature (Truesdell, 1974) to 8.5 ppt at 450 °C; fractionation between liquid CO_2 and water is the same to within 1 ppt (Rosenbaum, 1993) and those between water and either the carbonate or bicarbonate ions are smaller (Beck and others, 2005). All these cited equilibria were measured at 1 bar and little has been written about the effects of pressure. It has been reported that application of 2 GPa pressure on the system of $CaCO_3$ and water (at 500 °C) produced no change in the ^{18}O fractionation factor above the measurement uncertainty of 0.2 ppt (Clayton and others, 1975). Evaluation of this equilibrium at the maximum pressure of our current study (and room temperature, for which the effect, proportional to 1/T, is greatest) indicates that this upper limit would correspond to a maximum shift of <2 ppt, about an order of magnitude less than the effects of temperature, so we may assume the effect of pressure to be relatively small. Considering both pressure and temperature effects, it is therefore assumed that the (unknown) fractionation will not exceed several tens of ppt. In order to obviate the effects of fractionation we used amounts of doping far in excess of these variations.

At low X_{CO2} the isotopic content of the equilibrated water is minimally altered by exchange with the initial CO_2 and thus its contribution to the isotopic content of the CO_2, and the contribution of the fractionation factor to the uncertainty, is greatest. For a load with $X_{CO2} = 20$ percent, an uncertainty of as much as 40 ppt in the fractionation factor (assumed due mostly to a lack of knowledge of the final temperature of equilibration) would lead to an error of 3 percent absolute in calculated concentration. In our calculations we use as the fractionation factor the room temperature value for CO_2 over liquid water. With this presumption, an error of as much as 40 ppt is improbable as we may reasonably presume that the final distribution of isotopes is not governed by the highest temperature achieved in the experiments, but rather that equilibration is locked in as the cell load solidifies upon cooling. Since we lower the pressure before the 160 °C bake-out, the relevant temperature will be somewhere between the liquidus and solidus of CO_2-saturated water around 2 GPa, thus less than 100 °C. The fractionation of ^{17}O between CO_2 and water was assumed to be half that between ^{18}O and water (Craig, 1957; Barkan and Luz, 2012). The adequacy of the foregoing assumptions is borne out by the experimental results.

Calculation of mole fractions.—Given the known, initial isotopic compositions of both the aqueous solution and the liquid carbon dioxide, and presumed fractionation factors, the fractional amounts $^{13}C/C_{total}$, $^{17}O/O_{total}$ and $^{18}O/O_{total}$ in the resulting, equilibrated CO_2 (P_{13}, P_{17} and P_{18}, respectively) could be calculated for any assumed mole fraction in a DAC load. In turn, these fractional amounts allow calculation of the expected ratio of the ion current at 45 amu to that at 44 amu as:

$$R_{45/44} = [P_{13}(1 - P_{18} - P_{17})^2 + 2(1 - P_{13})(1 - P_{18} - P_{17})P_{17}]/[(1 - P_{13})(1 - P_{18} - P_{17})^2] \quad (1a)$$

and that of 46 to 44 amu as:

$$R_{46/44} = [2(1 - P_{13})(1 - P_{18} - P_{17})P_{18} + 2P_{13}(1 - P_{18} - P_{17})P_{17} + (1 - P_{13})P_{17}^2]/[(1 - P_{13})(1 - P_{18} - P_{17})^2] \quad (1b)$$

For each load, $R_{45/44}$ and $R_{46/44}$ were measured and values of X_{CO2} were sought that individually satisfied each of the two equations. Concurrence of the two values was taken to indicate a probable correct analysis of the DAC contents.

In order to test our procedure, small aliquots of the working aqueous solution were added to flasks of gaseous carbon dioxide, to produce mole fractions spanning 10 to 85 percent CO_2. After equilibration for several days, the flasks were placed first into liquid nitrogen, then into a slush at −78 °C. Samples of the gas, in amounts roughly equivalent to those expected in a typical DAC load (2 μL at 1 bar), were drawn off with a gas-tight syringe. These were then injected into the DAC extraction system through an auxiliary septum and analyzed in the manner described for DAC loads. With good bake-out procedure, the measured X_{CO2} was accurate to better than 1 percent absolute, for both isotopic gauges.

Precision and accuracy of measured mole fractions.—Mole fractions of DAC contents determined for the earlier of our experiments are less reliable than those of the later runs, with results from ^{18}O typically giving a larger X_{CO2} than from the simultaneous ^{13}C measurements. Three likely sources of error are 1. oxygen exchange with water (or other sources of oxygen) in the extraction system, which would tend to decrease the amount of ^{18}O and thus increase the apparent X_{CO2} as indicated by that isotope, 2. aspiration of small crystals of bicarbonate into the load upon re-opening the cell inside the liquid CO_2, which would increase the amount of ^{13}C and thus decrease the apparent X_{CO2} as indicated by ^{13}C, and 3. rapid isotope exchange during the few seconds a cell is open inside the liquid CO_2, followed by expulsion of part of the fluids during closure.

During the course of the experiments it became apparent that determinations of X_{CO2} based on ^{18}O were usually consistent with each other and could provide a smooth miscibility surface, while those based on ^{13}C not only were often shifted to lower values, but were also more scattered. Our understanding of the likely sources of errors, and the systematics of the results, indicated that simply rinsing the cell directly after loading with solution was inadequate. Further methods (acid bath, ultrasonification, filling cavities with gold), as described above, as well as longer periods of bake-out, were progressively undertaken with the result that the ^{13}C and ^{18}O measurements converged to a rms deviation of 4 percent absolute or, barring one outlier, 2.5 percent (calculated for the last 16 measurements).

A better appreciation of the precision, and perhaps accuracy, of the current measurements can be achieved by considering the limiting pressures of immiscibility of those loads with $X_{CO2} < 40$ percent (see Results, below). When plotted against X_{CO2} as measured by either ^{18}O or ^{13}C (fig. 5), these pressures can reasonably be fit to straight lines with rms deviation of 2 percent in X_{CO2}. Across the span of these data the best-fit lines for the two isotopes differ by less than 0.8 percent in X_{CO2}.

Acquired Data

Compositions explored.—In all we have investigated 30 different DAC loads, 26 of them with isotopic doping (table 1). The loads may be categorized into three types: 1. eighteen for which X_{CO2} as measured by ^{13}C and by ^{18}O agree to within 4 percent (mostly later data) and together define a smooth miscibility surface. 2. those with ^{18}O a

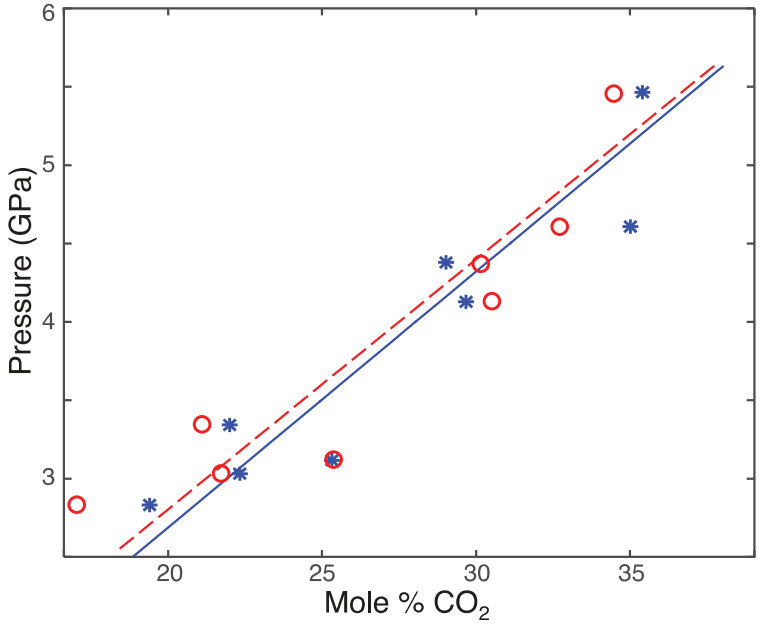

Fig. 5. The maximum pressure at which two fluid phases can co-exist (see, Results) is plotted against X_{CO2}, the latter measured by ^{18}O (*) and ^{13}C (o) content, with solid and dashed straight line fits to the two, respectively. Mole fractions exhibit a rms deviation of 2% from the lines, and a maximum outlier of 3%. All points with X_{CO2} <40% are plotted; most derive from the later, more fastidious, loading and purging techniques.

likely close upper bound in X_{CO2} but incompatible ^{13}C results ranging from 4 to 27 percent lower. There are six of these, most acquired before taking steps to reduce ingress of salt dust. 3. two sets of data (from the earliest runs) for which we suspect the ^{18}O to be in serious error, and four without isotopic doping. For these six sets only the shapes and positions of the homogenization curves are considered of importance. X_{CO2} for the two outlying, doped samples have been estimated from comparison with the other data and are given parenthetically in table 1. All observed points of homogenization are tabulated as Supplementary Data (http://earth.geology.yale.edu/%7eajs/SupplementaryData/2017/Abramson).

The data sets taken in the absence of isotopic doping, and thus in the absence of added salt, do not demonstrate noticeably different behavior from those with 0.055 mol-kg^{-1} $NaHCO_3$. In particular, three such sets exhibit the same pressure/temperature limit along what has been identified as the critical curve (see fig. 6B). In these three, early experiments, one of the cells had the usual rhenium gasket lined with gold, one of rhenium without liner, and another a gasket of Hastelloy C-276 which suffered increasing, visible corrosion over the course of the measurements. It may reasonably be inferred that the critical temperatures, and probably the balance of the data, were unaffected by either the deliberately added bicarbonate or any possible products of corrosion.

Temperature-pressure traces.—In figure 6, pressures and temperatures of homogenization are plotted for 21 compositions, chosen to display the full range of X_{CO2}. A typical load is initially solid at room temperature, producing fluid when warmed. As an example, and with reference to figure 6A, consider a load with X_{CO2} = 19 percent, warmed from an initial temperature of 20 °C while constrained to a 2.0 GPa isobar. (In

TABLE 1

X_{CO2} as determined by ^{13}C and by ^{18}O (values suggested by the fitted surface are given parenthetically for two outliers)

Run #	X_{C02} (%) by ^{13}C	X_{C02} (%) by $^{18}0$	data type
1	41	45	1*
2	75	89	2
3	25	43 (35)	3
4	28	51 (28)	3
5	62	89	2*
6	41	49	2
7	64	68	1
8	17	19	1*
9	54	63	2*
10	67	69	1*
11	63	69	2*
12	48	49	1*
13	90	92	1*
14	44	43	1
15	22	22	1*
16	31	30	1*
17	61	57	1*
18	88	90	1*
19	78	91	2
20	21	22	1*
21	35	35	1*
22	33	35	1*
23	56	53	1*
24	61	60	1*
25	30	29	1
26	25	25	1

* Plotted in figure 6.

actual practice, for a nearly isochoric sample chamber, pressure rises only modestly with increasing temperature, with larger increases during melting transitions.) When the sample reaches 65 °C, the water (ice VI) melts to produce a H_2O-rich fluid with a eutectic concentration achieved by the concomitant dissolution of solid CO_2 (Abramson, 2017). Above 65 °C, solid CO_2 continues to dissolve into the aqueous fluid owing to its increasing solubility. At 161 °C, the remaining solid CO_2 melts to produce a second, CO_2-rich fluid which is immiscible with the H_2O-rich fluid still present. Further increase in temperature results in the two fluids dissolving into each other and finally, at 275 °C, only a single, homogeneous fluid remains. Repeating the experiment at different starting pressures yields additional pressure-temperature points of homogenization, which together define the surface of miscibility at this composition of X_{CO2} = 19 percent. When lowering the temperature, fluid-fluid de-homogenization can often be followed into a region in which the majority-CO_2 fluid is metastable with respect to precipitation of solid CO_2, providing points on the low temperature side of the CO_2 melting line.

RESULTS

Observed Progressions in the Temperature-Pressure Traces

The lowest pressure of our experiments was 400 MPa, just slightly higher than the saddle point evident from the data of Todheide and Franck, 1963, or of Takenouchi

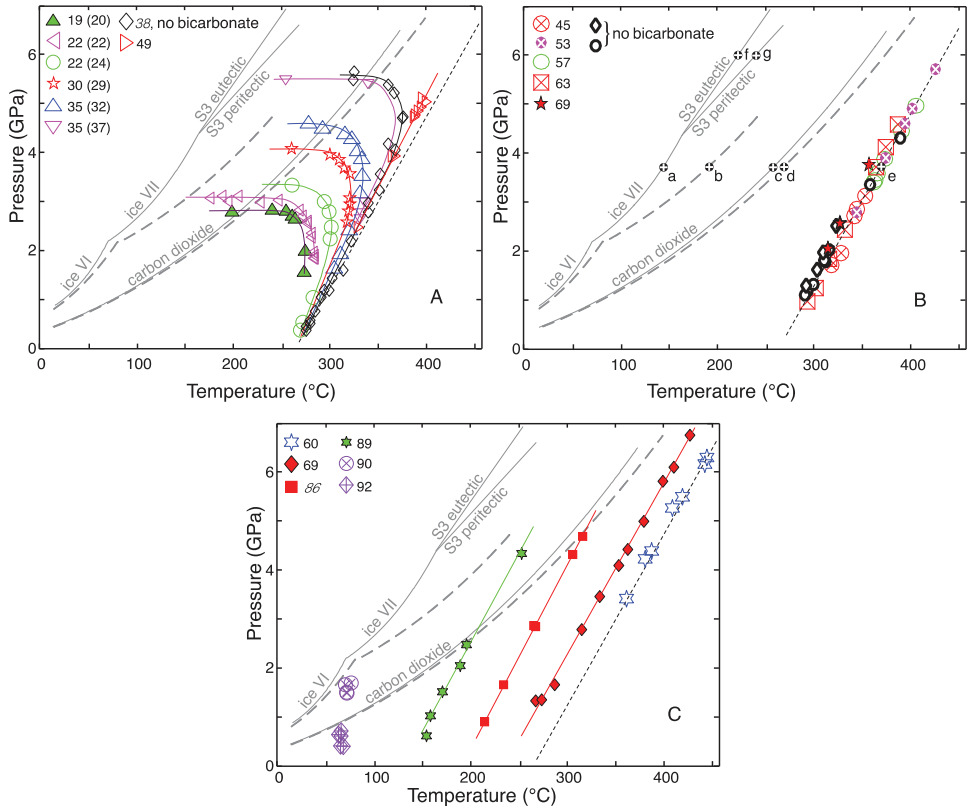

Fig. 6. Pressures of homogenization are plotted against temperature for 21 DAC loads. For each panel, numbers in the legends give X_{CO2} in mole percent as determined solely from ^{18}O content; two italicized numbers give best estimates in the absence of isotopic data. As well, melting curves of water and CO_2 are given for the pure compounds (long dashed lines, Wagner and others, 1994; Datchi and others, 2000; Abramson, 2017), the corresponding CO_2- or water-saturated solutions (solid lines, Bollengier and others, 2013; Abramson, 2017) and, above 4.4 GPa, the S3-H_2O(VII)-fluid eutectic and S3-CO_2(I)-fluid peritectic (solid lines, Abramson and others, 2017). Filled circles overlaid with "+" and labeled from "a" to "g" refer to points shown in figure 12. The straight line with short dashes indicates a best fit through points associated with visually observed critical behavior (eq 2). (A) Eight different DAC loads at low values of X_{CO2} show a progression of back-hooked curves which approaches the pressure-temperature locus of the critical curve. For these curves, values of X_{CO2} which can also be calculated from figure 5 are given parenthetically. (B) Traces from seven loads with X_{CO2} between 45 and 70% line up near the critical curve, evidencing a slow variation of the miscibility surface in the region around the critical concentrations. (C) As X_{CO2} increases beyond the critical concentrations the curves appear as straight lines, at progressively lower temperatures.

and Kennedy, 1964; as expected from these previous works, the temperatures of homogenization (T_h) initially increase with pressure (fig. 6) when observed along the compositional isopleths of individual DAC loads. For systems with $X_{CO2} < 40$ percent (fig. 6A), after this initial increase, T_h reaches a maximum (for example, 275 °C at 2 GPa for $X_{CO2} = 19\%$), declines, and then drops abruptly along a good approximation to an isobar. Above the pressure at which the drop occurs (2.8 GPa for $X_{CO2} = 19\%$) only a single fluid phase exists. This limiting pressure increases as X_{CO2} increases (figs. 5 and 6A). At higher concentrations of carbon dioxide (figs. 6B and 6C) the temperature reversal, if it occurs, has not been observed, while for $X_{CO2} \geq 86$ percent it is clearly disallowed by the freezing out of solid CO_2(I).

If, instead, we were able to increase the CO_2 content along an isobar we would observe first an increasing T_h (back-hooked traces in fig. 6A), followed by a plateau

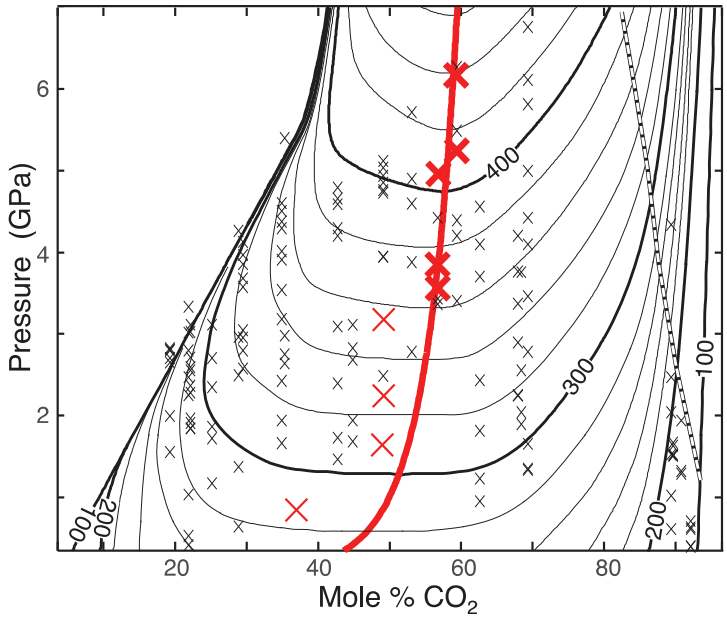

Fig. 7. Temperature contours (°C) of the calculated miscibility surface are plotted at intervals of 20 °C against mole fraction carbon dioxide and pressure. Small (black) crosses denote points at which de-homogenization was observed. Larger (red) crosses denote points at which near-critical behavior was observed, with the thicker of these pertaining to critical opalescence (fig. 3) and the thinner to the rapid movement and collapse of larger bubbles. An estimate of the critical curve is given by the thick (red) curve. The dashed curve indicates where, on the side of high X_{CO2}, the surface crosses the univariant freezing line of water-saturated carbon dioxide; at low X_{CO2} the same pressure-temperature locus lies in the region of closely spaced contours (and is not indicated).

with relatively constant T_h over a broad compositional range (fig. 6B), and finally a decrease (linear traces in figure 6C). Thus, the single-fluid regime is entered at relatively low temperature for loads of either small or large X_{CO2}, while loads with X_{CO2} between 45 and 70 percent homogenize along substantially the same, higher temperature. The point in this progression for which $(\partial T_h/\partial X_{CO2})_P = 0$ defines the critical curve at the pressure of that isobar. The pressure-temperature coordinates of the critical curve are manifested as the pronounced, high temperature limit of the combined de-homogenization curves (short dashed line in fig. 6) and are measureable independent of a knowledge of concentrations. With further pressure increase, the fluid-fluid critical temperature might fall below the freezing point of water-saturated CO_2, which would result in an upper critical endpoint. Above that pressure, only solids and/or a single fluid would exist. However, this has not yet been observed and, as shown in figure 6, the freezing line of water-saturated CO_2 trends away from that of pure CO_2 with increasing pressure, which slows its approach to the critical curve.

Miscibility Surface

The data can be used to construct the surface of miscibility, $T_h(X_{CO2}, P)$, shown in the contour plot of figure 7 and tabulated as Supplementary Data (http://earth.geology.yale.edu/%7eajs/SupplementaryData/2017/Abramson). Mole fractions were taken as determined by measurements of ^{18}O from data types 1 and 2. The surface between X_{CO2} = 70 percent and 90 percent, where we have only one set of data (without a determination of X_{CO2}), has been interpolated. In this region we

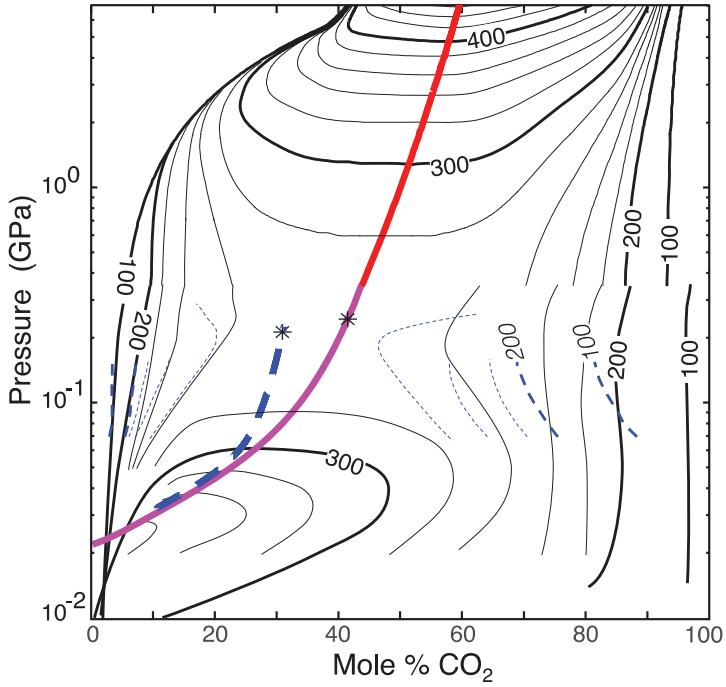

Fig. 8. Temperature contours (°C) of the calculated miscibility surface are plotted against mole fraction carbon dioxide and pressure. Above 350 MPa the surface is based on data from this study; the thicker (red) line indicates the critical curve. Contours (solid, black lines) below 350 MPa follow the data of Todheide and Franck, 1963, with the critical curve given as a thick, solid (magenta) line. Dashed (blue) contours and italicized temperatures represent some of the data of Takenouchi and Kennedy, 1964, with their estimate of the critical curve given by the thick, dashed (blue) line. Asterisks mark the saddle point as determined by these two previous studies.

constrained $(\partial T_h/\partial P)_{XCO2}$ to be constant for any value of X_{CO2} as is required by the straight pressure-temperature traces.

Surfaces drawn from both our new data and previous, lower pressure, work are shown together in figure 8 with a logarithmic pressure scale. Overall, as pressure rises, the maximum temperature of de-homogenization is seen first to descend from the critical point of pure water to the previously noted saddle point and then to rise again, while the associated value of X_{CO2} consistently increases. It is indicative of the rapidly varying nature of the fluids that a mixture with X_{CO2} = 30 percent, when held at 300 °C, is homogeneous at 10 MPa, but then with increasing pressure de-homogenizes at 15 MPa, re-homogenizes at 60 MPa, de-homogenizes again at 1.6 GPa and once again homogenizes at 4.2 GPa, just before the precipitation of solid CO_2 (at 4.6 GPa).

Comparison of overlapping data sets.—In constructing the miscibility surface of figures 7 and 8, the data of Todheide and Franck, 1963, taken at 350 MPa were used only for values of X_{CO2} less than 30 percent, in which range their data were not inconsistent with ours. At higher X_{CO2} the two data sets are not in agreement. Similarly, the studies of Todheide and Franck, 1963, are in reasonable agreement with those of Takenouchi and Kennedy, 1964, for lower X_{CO2} (and lower pressures), but the two differ significantly above approximately X_{CO2} = 50 percent. Subsequent work of Mather and Franck, 1992, determined homogenization curves with individual loads of constant, known composition (as in this study) in place of sampling the two fluids at a variety of P-T conditions as in the previous two studies. The substantial agreement with

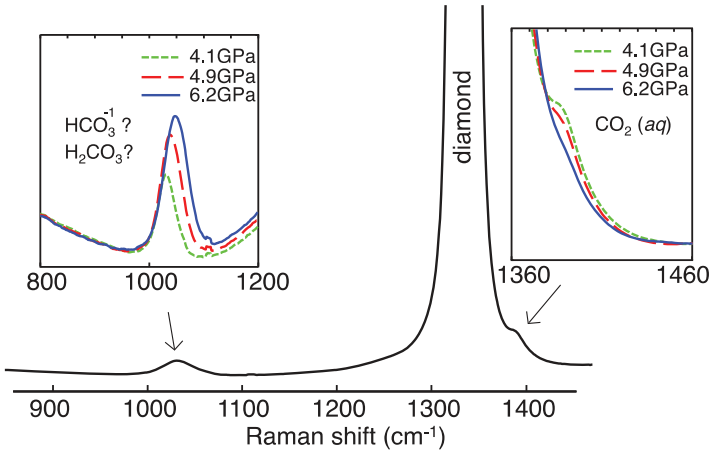

Fig. 9. Raman spectra of a 26 mole% solution at 250 °C. The line at ~1390 cm^{-1} is due to dissolved, aqueous CO_2; as pressure is raised, this line is seen to disappear while another line appears at ~1040 cm^{-1}.

the work of Todheide and Franck, 1963, was used to argue that their determination of sample contents was correct. A single point at 300 MPa, the highest pressure reported by Mather and Franck, 1992, did not fit the previous data and was hypothesized to indicate systematic error in the results of Todheide and Franck, 1963, at pressures above the saddle point. The only near overlap of any of those high-X_{CO2} data with ours is at our points around 400 MPa, 66 °C and X_{CO2} = 92 percent. A short extrapolation from the highest pressure of 350 MPa in Todheide and Franck, 1963, predicts at the same pressure and temperature a fluid with X_{CO2} >98 percent. The section of pressure-temperature-composition space in which these points occur is at the furthest extent of both experiments, was covered neither by Takenouchi and Kennedy, 1964, nor by Mather and Franck, 1992, and the discrepancy remains unresolved.

DISCUSSION

Speciation

In figure 7, and the upper part of figure 8, the edge of closely spaced contours on the side of low X_{CO2} corresponds to those sections of the pressure-temperature traces in figure 6A which are seen to hook back to lower temperatures. This large plunge in the temperature necessary for complete miscibility is believed to result from a correspondingly large, pressure-driven shift in speciation of the dissolved CO_2. Raman spectra taken in a 26 mol percent solution (fig. 9) show that as pressure is raised a peak associated with the solvated CO_2 molecule disappears and is replaced by another due to a different species. Since at higher pressures the original $CO_2(aq)$ peak is absent, we may conclude that such a H_2O-CO_2 fluid no longer contains carbon dioxide as the solvated molecular species.

What species is responsible for the new peak is not yet known. One obvious possibility is the bicarbonate ion. To explore this hypothesis, we used a modified Helgeson-Kirkham-Flowers theory (Shock and others, 1992) to carry out rough calculations of the $CO_2(aq)$ - bicarbonate equilibrium. At 250 °C, the ratio of the activity of bicarbonate to that of $CO_2(aq)$ was found to increase with pressure, reaching a value of 1 at roughly 4.7 GPa, close to the pressure at which figure 9 shows roughly half the $CO_2(aq)$ to have been replaced. Thermodynamic parameters used in the calculations were derived from measurements of the bicarbonate-carbonate equilibrium at

comparable pressures, coupled with extrapolation of lower-pressure parameters for $CO_2(aq)$ (Facq and others, 2014), while the dielectric constant of the fluid was approximated as that of water (Sverjensky and others, 2014b). That last approximation is particularly problematic; for example, if all the CO_2 were to be dissolved as $CO_2(aq)$ the dielectric constant would be greatly reduced, from a value of 66 to roughly 27 (Looyenga, 1965) and the pressure at which $CO_2(aq)$ and bicarbonate achieve equal activity increased by 1 GPa ; the effect of dissolution as an ionic species is more complicated to estimate but appears to be of roughly comparable magnitude (Gavish and Promislow, 2016, and examples therein). Given the uncertainties of the CO_2 parameters, the dielectric constant, and the activity coefficients at the large concentrations of our experiment, the coincidence between calculation and observation is encouraging, but not conclusive.

The Raman shift of the new line is 20 cm^{-1} larger than that reported for the expected bicarbonate ion at an equivalent pressure (Facq and others, 2014) and, while this discrepancy may be due to solvent effects associated with the much higher concentrations in our solution, the same line in a similar solution has been attributed (Wang and others, 2016) to the equivalent C-O stretch of dissolved carbonic acid. Further, a new solid phase of the H_2O-CO_2 system becomes thermodynamically favored at pressures above 4.4 GPa (Abramson and others, 2017); if this solid is composed of a new chemical species, possibly carbonic acid, it might be expected to be found also in solution. Further Raman studies, in solutions of varied concentration, or with a solvent composed of 50 percent D_2O, are expected to resolve this question.

It was noted by Facq and others, 2014, that while it is commonly assumed that CO_2(aq) is the dominant carbonic species in aqueous solutions, this is not true at the higher temperature (400 °C), dilute, basic solutions with which they worked. Additionally, "first principles" molecular dynamics models (Pan and Galli, 2016) suggest that at 11 GPa and 1000K, dilute (X_{CO2} = 1.6%) solutions contain less than 1 percent of the carbon as molecular CO_2(aq), most of it existing as the bicarbonate ion and 10 to 20 percent as carbonic acid. From our experiments, we can now add that even at lower temperatures and more concentrated, acidic conditions, CO_2(aq) becomes a minor species at GPa pressures. As a consequence, any accurate thermodynamic description of the H_2O-CO_2 system requires that such speciation be taken into account, and simpler models are unlikely to be satisfactory across multiple regions of different speciation.

The geological importance of the solution chemistry of CO_2 has been emphasized by an unexpectedly large contribution of fluid-mediated carbonate removal found (Ague and Nicolescu, 2014) in the Cycladic subduction complex (Greece); in order to understand the large inferred solubilities it will undoubtedly be necessary to have a more complete understanding of the relevant speciation, particularly in the presence of co-solutes (see also, Manning, 2014), than contained in current geochemical models.

Comparison with Published Equations of State

A variety of equations of state for the H_2O-CO_2 system have been proposed in the literature, and used in various geophysical models. Among the more commonly cited are a modified Redlich-Kwong expression (Kerrick and Jacobs, 1981; Jacobs and Kerrick, 1981), highly parameterized virial expansions fit to combinations of low pressure data and higher pressure simulations (Duan and Zhang, 2006; Zhang and Duan, 2009; Zhang and Duan, 2010), and modified van Laar expressions for excess Gibbs energy (Aranovitch and Newton, 1999; Holland and Powell, 2003).

Miscibility surfaces as predicted by these representations were tested against our data. For each EOS, Gibbs energies were calculated on a grid of P, T and X. At each P and T the method of common tangents was used to locate a pair of X_{CO2} in equilibrium

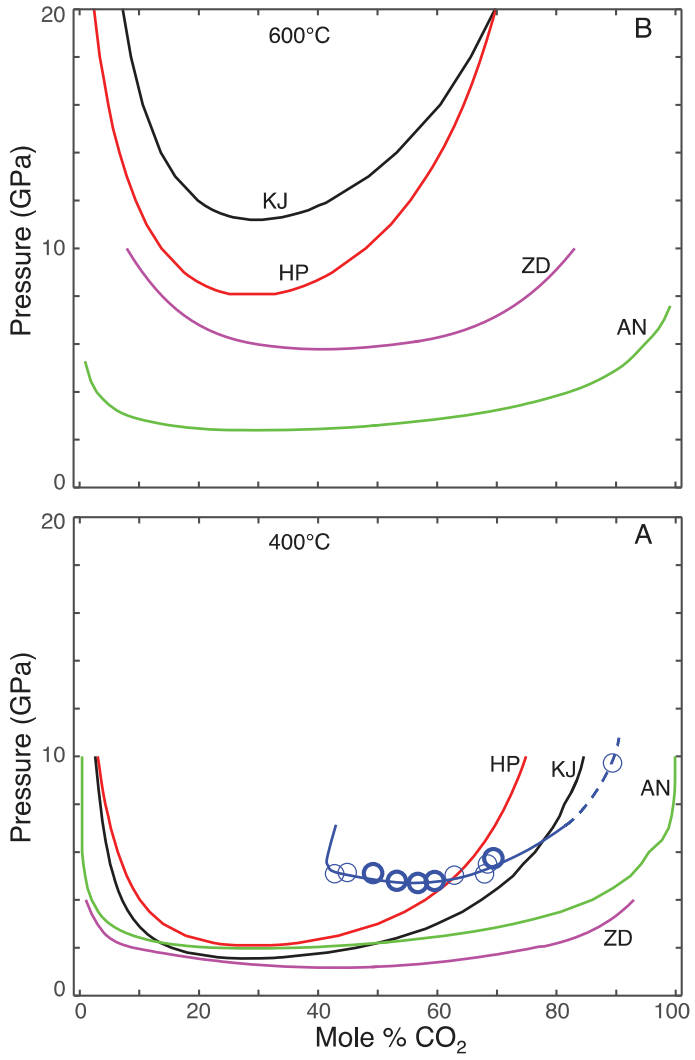

Fig. 10. P-X_{CO2} sections of the miscibility surface at (A) 400 °C and (B) 600 °C for several different EOS (Kerrick and Jacobs, 1981; Aranovich and Newton, 1999; Holland and Powell, 2003; Zhang and Duan, 2010). When the bulk composition lies on the concave side of such a curve (for a given P) two compositionally distinct fluids will exist. The thicker (blue) curve in the lower panel is from our current work (dashed portion extrapolated). Circles mark where compositions de-homogenize with increasing pressure; those drawn in thicker lines derive from P-T traces which spanned that pressure while thinner lines indicate extrapolations. As shown by our data, below a composition of X_{CO2} = 40% no de-homogenization occurs at 400 °C, at any pressure; this is due to a shift in speciation, a phenomenon not included in any of the models.

(if such existed), one corresponding to a relatively water-rich and the other to a CO_2-rich fluid. The totality of these pairs defines the miscibility surface. Isotherms through the surface (binodal curves) are plotted in figure 10 for 400 °C and 600 °C. At 400 °C (panel A), these EOS predict lower minimum pressures of immiscibility, and much wider compositional ranges, than observed. Those of Holland and Powell, 2003, and of Kerrick and Jacobs, 1981, which give a somewhat narrower compositional range of de-homogenization, have curves centered at ~30 percent, comparable to the lower pressure data of Takenouchi and Kennedy, 1964, but which fail to move to higher

X_{CO2} with higher pressure and temperature (as shown in panel B). [Note: Holland and Powell, 2003, give, and use, two different values for the interaction energy parameter; we have used a_{hc} = 10.5, which was optimized specifically for the CO_2-H_2O interaction.] Of the EOS tested, the exception is that of Duan and Zhang, 2006, (not to be confused with the later Zhang and Duan, 2009 and 2010) which errs in the contrary direction and, at 400 °C, predicts complete miscibility within its claimed limits of validity (P < 10 GPa).

At 600 °C the predicted binodal curves yield widely disparate minimum pressures of de-homogenization. Both KJ and HP indicate there to be significantly more water in the CO_2-rich fluid than CO_2 in the co-existing, water-rich fluid. All these EOS predict the solubility of CO_2 in water to be small over most, or all, of the range of de-homogenization; a slight increase in pressure would be expected to produce a dilute, aqueous fluid. The large solubilities of CO_2 into water, seen experimentally, are not consistent with the modelled thermodynamics.

As most of the data available to construct the above EOS were not in the pressure-temperature regime of the current experiments and, moreover, the prediction of de-homogenization is a sensitive test, it is perhaps not surprising that measured binodals are not reproduced. However, the extreme mismatch on the low X_{CO2} side is certainly caused by a failure to account for the shifting speciation. Thus, these EOS representations are not suitable as the basis for more complex models of COH fluids, including their saline solutions. Likewise, any molecular dynamics model that assumes CO_2 to exist as the intact, neutral molecule should not be expected to yield accurate results of the fluids' EOS (for example, Brodholdt and Wood, 1993; Destrigneville and others, 1996; Duan and Zhang, 2006), or their dielectric constants (Mountain and Harvey, 2015).

Critical Curve

The CO_2-H_2O system exhibits type III phase behavior (van Konynenburg and Scott, 1980), having two sections of critical curve. One section is extremely limited [7.38 ≤ P ≤ 7.411 MPa, (Wendland and others, 1999)] and pertains to a fluid and a gas, both closely approximating pure CO_2. The second section, of interest here, starts at the critical point of pure water (374 °C, 22 MPa) and continues beyond the highest pressures and temperatures of this study.

In figure 11 we plot the nine points at which critical or near-critical behavior was observed visually (figs. 3 and 7); a fit to these points (all located above 0.8 GPa) yields the equation:

$$P_{crit}(\text{GPa}) = 3.4 \times 10^{-2} \, (T_{crit}(^{\circ}\text{C}) - 270) + 0.35 \qquad (2)$$

with maximum deviation of 0.18 GPa. On the semilogarithmic scale of the figure they are seen to be in close alignment with the critical curve as tabulated by Todheide and Franck, 1963. As necessary, and seen in figure 6, this experimentally separate determination of the critical curve coincides with the high temperature limit of de-homogenization, $(\partial T_h / \partial X_{CO2})_P = 0$, along any given isobar.

While pressures and temperatures along the critical curve are well defined by our data, the miscibility surface does not peak sharply in X_{CO2}, being very broad, and so critical concentrations as determined by observations of homogenization are not as closely constrained. Although the fitted surface is consistent with the observed critical phenomena, the precise critical concentrations may be somewhat better determined by the latter.

In figure 10, the minimum pressure of each binodal defines a critical P-T-X point of the associated EOS. Such calculations can be repeated at different temperatures and the critical curves thus mapped out. These curves have been calculated for literature

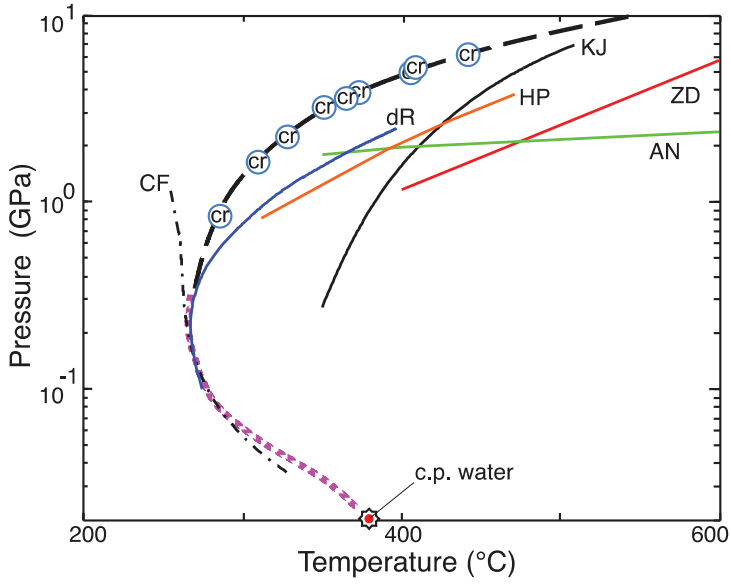

Fig. 11. Points at which (near)-critical behavior was seen are denoted by circles containing the letters "cr." The dashed line represents a fit through these points (eq 2) and, for a given pressure, can be seen (fig. 6) to coincide with the highest temperature at which two co-existing fluids are observed. The line of critical points tabulated in Todheide and Franck, 1963, is depicted as (magenta) dots, and terminates in the critical point of pure water (22 MPa and 374 °C). Also shown are critical curves given by various EOS (Kerrick and Jacobs, 1981; Christoforakos and Franck, 1986; Aranovich and Newton, 1999; Holland and Powell, 2003; dos Ramos and others, 2007; Zhang and Duan, 2010). For clarity the last curve is drawn in alternating dots and dashes. Duan and Zhang, 2006, predicts there to be no critical curve at temperatures within its stated range of applicability (>400°C and <10GPa).

EOS and their P-T traces are depicted in figure 11. Again, as previously seen in the binodals, most EOS require much lower pressures (or higher temperatures) for infinite miscibility than are determined experimentally. The exceptions are the EOS of Duan and Zhang, 2006, which predicts complete miscibility even at its highest pressure of applicability (10 GPa), and also of Christoforakos and Franck, 1986, which deviates to lower temperatures. Both this last EOS and one derived by dos Ramos and others, 2007, from Statistical Associating Fluid Theory (SAFT) were forced to conform to the experimentally determined values near the minimum in T_h, but diverge rapidly from measurements once beyond the region of previously available data.

Adding Solids to the Phase Diagram

Regions of fluid-fluid co-existence reported above can now be combined with previously reported solid-fluid and solid-solid equilibria to produce a fuller picture of the H_2O-CO_2 system, encompassing now also the pressure-temperature conditions found in small, icy worlds (Callisto, Europa, Ganymede and Titan, for example). T-X_{CO2} cross-sections of the phase diagram are shown in figure 12 at isobars of 1, 4 and 6 GPa. At these pressures, in addition to the fluid phases F1 and F2 (majority aqueous and majority CO_2, respectively), the solids H_2O(VI), H_2O(VII), and CO_2(I) can be present. Yet another crystalline phase, S3, is found to be in equilibrium with the aqueous fluid above a pressure of 4.4 GPa (Abramson and others, 2017); on the basis of Raman and IR spectra, this last phase has been suggested to be carbonic acid (Wang and others, 2016).

Pressures and temperatures of these various solid-fluid equilibria have been reported previously. The melting point of CO_2 into its water-saturated fluid (labeled

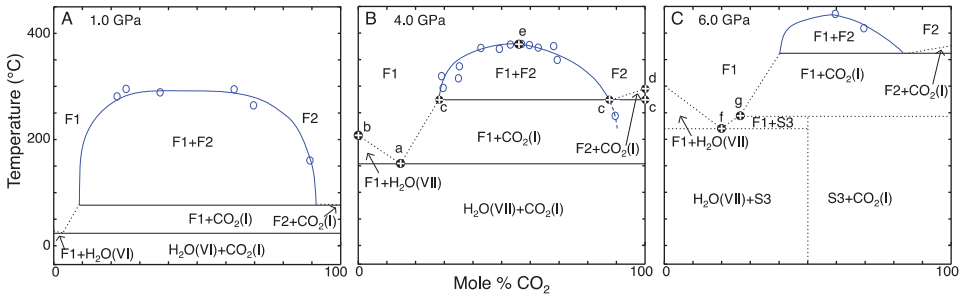

Fig. 12. T-X_{CO2} cross-sections at pressures of 1.0, 4.0 and 6.0 GPa. Regions of stability of two different fluids, solid water and solid CO_2, and a solid, H_2O-CO_2 compound (S3) are shown. A dashed extension of the fluid-fluid equilibrium surface indicates metastabilities. Open circles indicate temperatures of homogenization for various sample loads. In panel B the labels "a" through "e" refer, respectively, to the F1-H_2O(VII)-CO_2(I) eutectic equilibrium, the melting point of pure water, the F1-F2-CO_2(I) equilibrium, the melting point of pure CO_2 (which in this panel is exaggerated by 10 °C in order better to reveal the small region of under-saturated CO_2 fluid), and the critical point at this pressure. In panel C the labels "f" and "g" designate the F1-H_2O(VII)-S3 eutectic and F1-CO_2(I)-S3 peritectic. These labels correspond to those in fig. 6. X_{CO2} have not been measured for those phase boundaries denoted by dotted lines, nor for the eutectics or peritectic.

"c" in panel B), the F1-H_2O(VII)-CO_2(I) eutectic equilibrium ("a"), and the corresponding F1-H_2O(VI)-CO_2(I) eutectic at 1 GPa, as well as the melting curve of pure CO_2 ("d") all follow Simon-Glatzel curves (Abramson, 2017):

$$P = P_0 + a((T/T_0)^b - 1) \quad (3)$$

with parameters P_0, T_0, a and b given in table 2. The F1-H_2O(VII)-S3 eutectic and F1-CO_2(I)-S3 peritectic curves are given, respectively, by:

$$P(\text{GPa}) = 4.4 + 0.028\,(T(^\circ\text{C}) - 165) \quad (4a)$$

and:

$$P(\text{GPa}) = 4.4 + 0.021\,(T(^\circ\text{C}) - 165) \quad (4b)$$

Two CO_2 hydrates, a sI clathrate and a filled ice (Hirai and others, 2010; Bollengier and others, 2013; Tulk and others, 2014), exist only at pressures less than 1 GPa and are not shown in the figure.

The thermodynamic limit of the two-fluid regime due to the freezing of water-saturated CO_2 (point "c" in figure 12B) is also indicated on the surface of figure 7. With further pressure increase, the fluid-fluid critical temperature might fall below the freezing point of water-saturated CO_2, which would result in an upper critical endpoint. Above that pressure, only solids and/or a single fluid would exist. However, this

Table 2

Coefficients for equation (3) for various equilibria

	Po (GPa)	*To* (K)	*a* (GPa)	*b*
F1-H_2O(VI)-CO_2(I)	0.77	279	0.412	7.201
F1-H_2O(VII)-CO_2(I)	2.21	345	0.875	5.277
Pure CO_2(I) melt	0.00	216.59	0.451	2.444
F1-F2-CO_2(I)	0.00	216.59	0.404	2.588

has not yet been observed and, as shown in figure 6, the freezing line of water-saturated CO_2 trends away from that of pure CO_2 with increasing pressure, which slows its approach to the critical curve.

CONCLUSIONS

Fluid-fluid phase equilibria in the H_2O-CO_2 binary have been measured to pressures of 7 GPa and temperatures of 450 °C, extending our knowledge of this system to Earth mantle conditions, notably in convergent zones where old lithosphere is being rapidly subducted, and to the deep interiors of icy worlds. A miscibility surface has been constructed and the critical curve was determined. To the highest pressures achieved in this study, fluid-fluid immiscibility persists, and any imminent critical endpoint is not evident in the data; at the higher pressures, the rate at which the CO_2 liquidus approaches the critical curve diminishes.

Systems with mole fractions of CO_2 less than roughly 40 percent exhibit a maximum pressure of immiscibility, above which the fluids are completely miscible for all temperatures; this maximum increases with the mole fraction CO_2 in the system and is associated with a shift in speciation of CO_2. Raman spectra of the solution acquired at these conditions show a disappearance of CO_2(aq) and the simultaneous appearance of a new species, possibly bicarbonate or carbonic acid. It is clear that in large regions of pressure-temperature-composition space dissolved CO_2 does not exist as CO_2(aq), and current thermodynamic representations that assume CO_2(aq) are inadequate. These results may have significant geochemical implications, as the changing speciation of carbon in C-O-H fluids is also likely to alter the dielectric constants, particularly of fluids with high proportions of CO_2, and thus the solubility and chemical potentials of other dissolved species.

Since water and carbon dioxide are ubiquitous planetary components, calculations of equilibrium behavior of complex mixtures require accurate descriptions of their combined equation of state. No currently available equation of state provides a successful prediction of our data. Neither the pressure-temperature-composition dependence of the miscibility surface nor the temperature-pressure projection of the critical curve is correctly estimated. Thus, in a regime overlapping with planetary conditions, petrological predictions remain tenuous using standard thermodynamic models for complex rock-fluid systems.

ACKNOWLEDGMENTS

We thank Andy Schauer at the University of Washington Isolab for his guidance in the subtleties of isotopic measurements, Scott Temple for his help in the laboratory, and also Matthew Steele-MacInnis and another, anonymous, reviewer for suggestions that led to a more readable manuscript. Work herein was supported by the Department of Energy, contract DE-NA0001843, by NASA Outer Planets Research grant NNX13AL23G and by the Icy Worlds node of NASA's Astrobiology Institute (13-13NAI7_2-0024).

REFERENCES

Abers, G. A., Nakajima, J., van Keken, P. E., Kita, S., and Hacker, B. R., 2013, Thermal–petrological controls on the location of earthquakes within subducting plates: Earth and Planetary Science Letters, v. 369–370, p. 178–187, https://doi.org/10.1016/j.epsl.2013.03.022

Abramson, E. H., 2017, Three-Phase Melting Curves in the Binary System of Carbon Dioxide and Water: Madrid, Spain, Joint 25th AIRAPT International Conference/EHPRG Meeting on High Pressure Science and Technology: Journal of Physics: Conference Series.

Abramson, E. H., Bollengier, O., and Brown, J. M., 2017, Water-carbon dioxide solid phase equilibria at pressures above 4 GPa: Scientific Reports, v. 7, 821, https://doi.org/10.1038/s41598-017-00915-0

Ague, J. J., and Nicolescu, S., 2014, Carbon dioxide released from subduction zones by fluid-mediated reactions: Nature Geoscience, v. 7, p. 355–360, https://doi.org/10.1038/ngeo2143

Andersen, T., and Neumann, E.-R., 2001, Fluid inclusions in mantle xenoliths: Lithos, v. 55, n. 1–4, p. 301–320, https://doi.org/10.1016/S0024-4937(00)00049-9

Aranovich, L. Y., and Newton, R. C., 1999, Experimental determination of CO_2-H_2O activity-composition relations at 600–1000 °C and 6–14 kbar by reversed decarbonation and dehydration reactions: American Mineralogist, v. 84, n. 9, p. 1319–1332, https://doi.org/10.2138/am-1999-0908

Audet, P., Bostock, M. G., Boyarko, D. C., Brudzinski, M. R., and Allen, R. M., 2010, Slab morphology in the Cascadia fore arc and its relation to episodic tremor and slip: Journal of Geophysical Research-Solid Earth, v. 115, n. B4, B00A16, https://doi.org/10.1029/2008JB006053

Barkan, E., and Luz, B., 2012, High-precision measurements of $^{17}O/^{16}O$ and $^{18}O/^{16}O$ ratios in CO_2: Rapid Communications in Mass Spectrometry, v. 26, n. 23, p. 2733–2738, https://doi.org/10.1002/rcm.6400

Beck, W. C., Grossman, E. L., and Morse, J. W., 2005, Experimental studies of oxygen isotope fractionation in the carbonic acid system at 15°, 25°, and 40 °C: Geochimica et Cosmochimica Acta, v. 69, n. 14, p. 3493–3503, https://doi.org/10.1016/j.gca.2005.02.003

Bodnar, R. J., Burnham, C. W., and Sterner, S. M., 1985, Synthetic fluid inclusions in natural quartz. III. Determination of phase equilibrium properties in the system H_2O-NaCl to 1000 °C and 1500 bars: Geochimica et Cosmochimica Acta, v. 49, n. 9, p. 1861–1873, https://doi.org/10.1016/0016-7037(85)90081-X

Bollengier, O., Choukroun, M., Grasset, O., Le Menn, E., Bellino, G., Morizet, Y., Bezacier, L., Oancea, A., Taffin, C., and Tobie, G., 2013, Phase equilibria in the H_2O–CO_2 system between 250–330 K and 0–1.7 GPa: Stability of the CO_2 hydrates and H_2O-ice VI at CO_2 saturation: Geochimica et Cosmochimica Acta, v. 119, p. 322–339, https://doi.org/10.1016/j.gca.2013.06.006

Brodholt, J., and Wood, B., 1993, Molecular dynamics simulations of the properties of CO_2-H_2O mixtures at high pressures and temperatures: American Mineralogist, v. 78, n. 5–6, p. 558–564.

Capobianco, R., Gruszkiewicz, M. S., Wesolowski, D. J., Cole, D. R., and Bodnar, R. J., 2013, Volumetric properties and fluid phase equilibria of CO_2 + H_2O: Stanford, California, Stanford University, Proceedings, Thirty-Eighth Workshop on Geothermal Reservoir Engineering, February 11–13.

Clayton, R. N., Goldsmith, J. R., Karel, K. J., Mayeda, T. K., and Newton, R. C., 1975, Limits on the effect of pressure on isotopic fractionation: Geochimica et Cosmochimica Acta, v. 39, n. 8, p. 1197–1201, https://doi.org/10.1016/0016-7037(75)90062-9

Costantino, M., and Rice, S. F., 1991, Supercritical phase separation in H_2O-N_2 mixtures: Journal of Physical Chemistry, v. 95, n. 23, p. 9034–9036, https://doi.org/10.1021/j100176a004

Craig, H., 1957, Isotopic standards for carbon and oxygen and correction factors for mass-spectrometric analysis of carbon dioxide: Geochimica et Cosmochimica Acta, v. 12, n. 1–2, p. 133–149, https://doi.org/10.1016/0016-7037(57)90024-8

Christoforakos, M., and Franck, E. U., 1986, An equation of state for binary fluid mixtures to high temperatures and high pressures: Berichte der Bunsen-Gesellschaft fuer Physikalische Chemie, v. 90, n. 9, p. 780–789. https://doi.org/10.1002/bbpc.19860900905

Datchi, F., Loubeyre, P., and LeToullec, R., 2000, Extended and accurate determination of the melting curves of argon, helium, ice (H_2O), and hydrogen (H_2): Physical Review B, v. 61, p. 6535–6546, https://doi.org/10.1103/PhysRevB.61.6535

Destrigneville, C. M., Brodholt, J. P., and Wood, B. J., 1996, Monte Carlo simulation of H_2O-CO_2 mixtures to 1073.15 K and 30 kbar: Chemical Geology, v. 133, n. 1–4, p. 53–65, https://doi.org/10.1016/S0009-2541(96)00069-1

Dos Ramos, M. C., Blas, F. J., and Galindo, A., 2007, Phase Equilibria, Excess Properties, and Henry's Constants of the Water + Carbon Dioxide Binary Mixture: Journal of Physical Chemistry C, v. 111, n. 43, p. 15924–15934, https://doi.org/10.1021/jp073716q

Duan, Z., and Zhang, Z., 2006, Equation of state of the H_2O, CO_2, and H_2O–CO_2 systems up to 10 GPa and 2573.15 K: Molecular dynamics simulations with *ab initio* potential surface: Geochimica et Cosmochimica Acta, v. 70, n. 9, p. 2311–2324, https://doi.org/10.1016/j.gca.2006.02.009

Eggler, D. H., Kushiro, I., and Holloway, J. R., 1979, Free energies of decarbonation reactions at mantle pressures: I. Stability of the assemblage forsterite-enstatite-magnesite in the system MgO-SiO_2-CO_2-H_2O to 60 kbar: American Mineralogist, v. 64, n. 3–4, p. 288–293.

Facq, S., Daniel, I., Montagnac, G., Cardon, H., and Sverjensky, D. A., 2014, *In situ* Raman study and thermodynamic model of aqueous carbonate speciation in equilibrium with aragonite under subduction zone conditions: Geochimica et Cosmochimica Acta, v. 132, p. 375–390, https://doi.org/10.1016/j.gca.2014.01.030

Frost, B. R., and Frost, C. D., 2014, Essentials of Igneous and Metamorphic Petrology: Cambridge, Cambridge University Press, 314 p.

Frost, D. J., and Wood, B. J., 1997, Experimental measurements of the properties of H_20-CO_2 mixtures at high pressures and temperatures: Geochimica et Cosmochimica Acta, v. 61, n. 16, p. 3301–3309, https://doi.org/10.1016/S0016-7037(97)00168-3

Gavish, N., and Promislow, K., 2016, Dependence of the dielectric constant of electrolyte solutions on ionic concentration: A microfield approach: Physical Review E, v. 94, 012611, https://doi.org/10.1103/PhysRevE.94.012611

Giordano, V. M., Datchi, F., and Dewaele, A., 2006, Melting curve and fluid equation of state of carbon dioxide at high pressure and high temperature: Journal of Chemical Physics, v. 125, n. 5, 054504, https://doi.org/10.1063/1.2215609

Harte, B., 2010, Diamond formation in the deep mantle: The record of mineral inclusions and their distribution in relation to mantle dehydration zones: Mineralogical Magazine, v. 74, n. 2, p. 189–215, https://doi.org/10.1180/minmag.2010.074.2.189

Hirai, H., Komatsu, K., Honda, M., Kawamura, T., Yamamoto, Y., and Yagi, T., 2010, Phase changes of CO_2

hydrate under high pressure and low temperature: Journal of Chemical Physics, v. 133, 124511, https://doi.org/10.1063/1.3493452
Hirschmann, M. M., and Dasgupta, R., 2009, The H/C ratios of Earth's near-surface and deep reservoirs, and consequences for deep Earth volatile cycles: Chemical Geology, v. 262, n. 1–2, p. 4–16, https://doi.org/10.1016/j.chemgeo.2009.02.008
Holland, T., and Powell, R., 2003, Activity–composition relations for phases in petrological calculations: An asymmetric multicomponent formulation: Contributions to Mineralogy and Petrology, v. 145, n. 4, p. 492–501, https://doi.org/10.1007/s00410-003-0464-z
Jacobs, G. K., and Kerrick, D. M., 1981, APL and FORTRAN programs for a new equation of state for H_2O, CO_2, and their mixtures at supercritical conditions: Computers and Geosciences, v. 7, n. 2, p. 131–143, https://doi.org/10.1016/0098-3004(81)90025-X
Kelemen, P. B., and Manning, C. E., 2015, Reevaluating carbon fluxes in subduction zones, what goes down, mostly comes up: Proceedings of the National Academy of Sciences of the United States of America, v. 112, p. E3997–E4006, https://doi.org/10.1073/pnas.1507889112
Kerrick, D. M., and Jacobs, G. K., 1981, A modified Redlich-Kwong Equation for H_2O, CO_2, and H_2O–CO_2 mixtures at elevated pressures and temperatures: American Journal of Science, v. 281, n. 6, p. 735–767, https://doi.org/10.2475/ajs.281.6.735
Looyenga, H., 1965, Dielectric constants of heterogeneous mixtures: Physica, v. 31, n. 3, p. 401–406, https://doi.org/10.1016/0031-8914(65)90045-5
Mader, U. K., 1991, H_2O-CO_2 mixtures: a review of *P-V-T-X* data and an assessment from a phase-equilibrium point of view: Canadian Mineralogist, v. 29, n. 4, p. 767–790.
Manning, C. E., 2014, A piece of the deep carbon puzzle: Nature Geoscience, v. 7, p. 333–334, https://doi.org/10.1038/ngeo2152
Mather, A. E., and Franck, E. U., 1992, Phase equilibria in the system carbon dioxide-water at elevated pressures: Journal of Physical Chemistry, v. 96, n. 1, p. 6–8, https://doi.org/10.1021/j100180a003
McCord, T. B., Hayne, P., Combe, J.-P., Hansen, G. B., Barnes, J. W., Rodriguez, S., Le Mouélic, S., Baines, E. K. H., Buratti, B. J., Sotin, C., Nicholson, P., Jaumann, R., Nelson, R., and the Cassini VIMS Team, 2008, Titan's surface: Search for spectral diversity and composition using the Cassini VIMS investigation: Icarus, v. 194, p. 212–242, https://doi.org/10.1016/j.icarus.2007.08.039
McLaren, E. H., and Murdock, E. G., 1960, The Freezing Points of High Purity Metals as Precision Temperature Standards: VI. Thermal analyses on five samples of lead with purities greater than 99.999+%: Canadian Journal of Physics, v. 38, n. 5, p. 577–587, https://doi.org/10.1139/p60-063
Mountain, R. D., and Harvey, A. H., 2015, Molecular dynamics evaluation of dielectric constant mixing rules of H_2O-CO_2 at geologic conditions: Journal of Solution Chemistry, v. 44, n. 11, p. 2179–2193, https://doi.org/10.1007/s10953-015-0401-6
Pan, D., and Galli, G. A., 2016, The fate of carbon dioxide in water-rich fluids under extreme conditions: Science Advances, v. 2, n. 10, e1601278, https://doi.org/10.1126/sciadv.1601278
Porco, C. C., Helfenstein, P., Thomas, P. C., Ingersoll, A. P., Wisdom, J., West, R., Neukum, G., Denk, T., Wagner, R., Roatsch, T., Kieffer, S., Turtle, E., McEwen, A., Johnson, T. V, Rathbun, J., Veverka, J., Wilson, D., Perry, J., Spitale, J., Brahic, A., Burns, J. A., DelGenio, A. D., Dones, L., Murray, C. D., and Squyres, S., 2006, Cassini observes the active south pole of Enceladus: Science, v. 311, n. 5766, p. 1393–1401, https://doi.org/10.1126/science.1123013
Poulton, D. J., and Baldwin, H. W., 1967, Oxygen exchange between carbonate and bicarbonate ions and water. I. Exchange in the absence of added catalysts: Canadian Journal of Chemistry, v. 45, n. 10, p. 1045–1050, https://doi.org/10.1139/v67-176
Rosenbaum, J. M., 1993, Room temperature oxygen isotope exchange between liquid CO_2 and H_2O: Geochimica et Cosmochimica Acta, v. 57, n. 13, p. 3195–3198, https://doi.org/10.1016/0016-7037(93)90303-E
Shadravan, A., and Amani, M., 2012, HPHT 101-What petroleum engineers and geoscientists should know about high pressure high temperature wells environment: Energy Science and Technology v. 4, n. 2, p. 36–60.
Shock E. L., Oelkers, E. H., Johnson, J. W., Sverjensky, D. A., and Helgeson, H. C., 1992, Calculation of the thermodynamic properties of aqueous species at high pressures and temperatures. Effective electrostatic radii, dissociation constants and standard partial molal properties to 1000 °C and 5 kbar: Journal of the Chemical Society, Faraday Transactions, v. 88, p. 803–826, https://doi.org/10.1039/FT9928800803
Sohl, F., Choukroun, M., Kargel, J., Kimura, J., Pappalardo, R., Vance, S., and Zolotov, M., 2010, Subsurface Water Oceans on Icy Satellites: Chemical Composition and Exchange Processes: Space Science Reviews, v. 153, n. 1–4, p. 485–510, https://doi.org/10.1007/s11214-010-9646-y
Sterner, S. M., and Bodnar, R. J., 1991, Synthetic fluid inclusions. X: Experimental determination of P-V-T-X properties in the CO_2-H_2O system to 6 kb and 700 °C: American Journal of Science, v. 291, n. 1, p. 1–54, https://doi.org/10.2475/ajs.291.1.1
Sverjensky, D. A., Harrison, B., and Azzolini, D., 2014b, Water in the deep Earth: The dielectric constant and the solubilities of quartz and corundum to 60 kb and 1200 °C: Geochimica et Cosmochimica Acta, v. 129, p. 125–145, https://doi.org/10.1016/j.gca.2013.12.019
Sverjensky, D. A., Stagno, V., and Huang, F., 2014a, Important role for organic carbon in subduction-zone fluids in the deep carbon cycle: Nature Geosciences, v. 7, p. 909–913, https://doi.org/10.1038/ngeo2291
Syracuse, E. M., Van Keken, P. E., and Abers, G. A., 2010, The global range of subduction zone thermal models: Physics of the Earth and Planetary Interiors, v. 183, n. 1–2, p. 73–90, https://doi.org/10.1016/j.pepi.2010.02.004

Takenouchi, S., and Kennedy, G. C., 1964, The binary system H_2O–CO_2 at high temperatures and pressures: American Journal of Science, v. 262, n. 9, p. 1055–1074, https://doi.org/10.2475/ajs.262.9.1055

Todheide, K., and Franck, E. U., 1963, Das Zweiphasengebiet und die kritische kurve in system kohlendioxide-wasser bis zu drucken von 3500 bar: Zeitschrift fuer Physikalische Chemie (Neue Folge), v. 37, p. 387–401, https://doi.org/10.1524/zpch.1963.37.5_6.387

Truesdell, A. H., 1974, Oxygen isotope activities and concentrations in aqueous salt solutions at elevated temperatures: Consequences for isotope geochemistry: Earth and Planetary Science Letters v. 23, n. 3, p. 387–396, https://doi.org/10.1016/0012-821X(74)90128-9

Tulk, C. A., Machida, S., Klug, D. D., Lu, H., Guthrie, M., and Molaison, J. J., 2014, The structure of CO_2 hydrate between 0.7 and 1.0 GPa: Journal of Chemical Physics, v. 141, 174503, https://doi.org/10.1063/1.4899265

Vance, S., Bouffard, M., Choukroun, M., and Sotin, C., 2014, Ganymede's internal structure including thermodynamics of magnesium sulfate oceans in contact with ice: Planetary and Space Science, v. 96, p. 62–70, https://doi.org/10.1016/j.pss.2014.03.011

van Hinsberg, M. G. E., Verbrugge, R., and Schouten, J. A., 1993, High temperature-high pressure experiments on H_2O-N_2: Fluid Phase Equilibria, v. 88, p. 115–121, https://doi.org/10.1016/0378-3812(93)87105-A

van Konynenburg, P. H., and Scott, R. L., 1980, Critical lines and phase equilibria in binary van der Waals mixtures: Philosophical Transactions of the Royal Society, A v. 298, n. 1442, p. 495–540, https://doi.org/10.1098/rsta.1980.0266

Vetter, G., 2001, Introduction, *in* Bertucco, A., and Vetter, G., editors, High Pressure Process Technology: Fundamentals and Applications: Amsterdam, Elsevier Science, Industrial Chemistry Library, v. 9, p. 1–15, https://doi.org/10.1016/S0926-9614(01)80019-8

Wagner, W., Saul, A., and Pruss, A., 1994, International equations for the pressure along the melting and along the sublimation curve of ordinary water substance: Journal of Physical and Chemical Reference Data, v. 23, n. 3, p. 515–527, https://doi.org/10.1063/1.555947

Wang, H., Zeuschner, J., Eremets, M., Troyan, I., and Willams, J., 2016, Stable solid and aqueous H_2CO_3 from CO_2 and H_2O at high pressure and high temperature: Scientific Reports, v. 6, 19902, https://doi.org/10.1038/srep19902

Wendland, M., Hasse, H., and Maurer, G., 1999, Experimental pressure-temperature data on three- and four-phase equilibria of fluid, hydrate, and ice phases in the system carbon dioxide-water: Journal of Chemical and Engineering Data, v. 44, n. 5, p. 901–906, https://doi.org/10.1021/je980208o

Zhang, C., and Duan, Z., 2009, A model for C–O–H fluid in the Earth's mantle: Geochimica et Cosmochimica Acta, v. 73, n. 7, p. 2089–2102, https://doi.org/10.1016/j.gca.2009.01.021

——— 2010, GFluid: An Excel spreadsheet for investigating C–O–H fluid composition under high temperatures and pressures: Computers and Geosciences, v. 36, n. 4, p. 569–572, https://doi.org/10.1016/j.cageo.2009.05.008